

The Effect of cathode Porosity on Solid Oxide Fuel Cell Performance

Authors

Mohammad Riazat^a
Majid Baniassadi^{a,b*}
Mohsen Mazrouie^a
Mehdi Tafazoli^c
Mahdi Moghimi Zand^a

^a School of Mechanical Engineering,
College of Engineering, University of
Tehran, P.O. Box 1155-4563, Tehran, Iran

^b University of Strasbourg, ICube/CNRS, 2
Rue Boussingault, 67000 Strasbourg,
France

^c Babol University of Technology, Shariati
Av., Babol, Mazandaran, Iran

ABSTRACT

In the present study, the effect of porosity on the cathode microstructure (50:50 wt. % LSM: YSZ) of a Solid Oxide Fuel Cell (SOFC) has been examined. A 3-D finite element method for Mixed Ionic and Electronic Conducting Cathodes (MIEC) is presented to study the effects of porosity on cell performance. Each microstructure was realized using the Monte Carlo approach with the isotropic type of growth rate. The effect of porosity on the cathode of a solid oxide fuel cell involving the Three Phase Boundary Length (TPBL), electric conductivity of LSM phase, ionic conductivity of YSZ, mechanical behavior and tortuosity of the pore phase were explored in the present work. The cathode having a porosity value between 31 and 34% revealed the maximum TPBL value as well as a high variation in the electrical conductivity of the LSM phase. Pore phase tortuosity was also decreased by increasing the porosity factor.

Article history:

Received : 4 November 2014

Accepted : 19 December 2014

Keywords: Fuel Cell, Microstructure, Material Design.

1. Introduction

Solid Oxide Fuel Cells (SOFC) is components used to generate electric energy via electrochemical reactions from renewable fuel or the chemical energy of fossils [1]. SOFCs can directly convert chemical energy into electrical energy with low emissions and high-efficiency [2], at an operating temperature of about 800°C. Reducing the operating temperature involves minimizing the electrode polarization resistances, especially that of the cathode [3]. Due to the high operating temperature, such fuel cells will be most appropriate in stationary applications such as power plants, ranging

from kW up to MW. One important benefit of the SOFCs compared with the low temperature fuel cells is their ability to consume not only hydrogen, but their ability to also use methane [4].

From several studies it is evident that composite cathodes with parallel pathway for electronic and ionic charge carriers have lower over potentials compared with the single-phase electrodes, which are composed of the electrocatalyst alone [5,6]. The SOFC technology is enhanced significantly with the composition of LSM–YSZ by providing reasonably low cathode polarization resistance [7-9]. The LSM and YSZ properties determine the cathode performance, which is also strongly dependent upon its microstructure [10]. The influence of the composite electrode microstructure on the electrochemical

*Corresponding author: Majid Baniassadi
Address : Assistant Professor, School of Mechanical Engineering, College of Engineering, University of Tehran, P.O. Box 1155-4563, Tehran, Iran
E-mail address: m.baniassadi@ut.ac.ir

performance was examined in some experimental studies [11-13]; however, they cannot be employed to obtain the best microstructure, because they are limited to a fewer microstructures which are evaluated at certain specific operating conditions.

All the electrochemical reactions of the cathode occur in the region of the boundaries shared among LSM, YSZ and the voids, which are termed Triple Phase Boundaries (TPB) [14]. The TPB significantly impacts the SOFC microstructure, which considerably controls its efficiency. Therefore, by designing a microstructure with the maximum TPB value through the best volume fractions for LSM, YSZ and voids, the cell performance can be increased [15].

Cell performance strongly depends on the electrode morphology, specifically on the actual conductivity of the phases and the morphological properties of the electrode related to the gas phase that are a function of composition, particle size, sintering conditions and porosity. The electrode porosity enables the gas to diffuse through the cell and the exhaust gas to escape from it [16]. This is controlled by the presence of the pore formers in the particle mixture. Pore formers are decomposable particles, which burn at high temperatures during sintering. Hence, the desirable porosity can be obtained by determining the portion of the pore former in the electrode mixture prior to sintering [17, 18]. Consequently, a clear understanding and optimization of the electrode morphology are essential in an engineered design.

Prior studies reveal that the electrochemical performance of the SOFCs is significantly affected by the electrode microstructure [8, 19]. Porosity is a distinctive factor of microstructure, which plays a significant role in cell performance [20]. In each microstructure having different porosity, the TPB value, mechanical behavior, pore phase tortuosity, electrical and ionic conductivity of the solid phase were examined and compared with each other.

2. 3-D Microstructure of the Cathode

In this work, the impact of porosity on TPB density, mechanical behavior, pore phase tortuosity and electrical conductivity of the SOFC cathode with different porosities ranging from 28, 31, 34, 37, 40 and 43% are investigated. The volume fraction of YSZ and LSM are considered with respect to earlier studies in which 50:50 weight % LSM: YSZ

has been reported to be the best volume fraction for the solid part [3,21]. The 3-D microstructures are realized by using the novel Monte Carlo approach, which involves three major steps including generation, distribution and cell growth rate.

In the first step, for different phases at some accidental nucleation points, several primary cells are placed. Based on an automaton algorithm of the cell, upon assignment of the initial cell geometries, the cell's growth begins. Realization steps are continued until the microstructure is achieved. Several virtual 3-D microstructures of a three-phase cathode have been realized by this approach. In the 3-D microstructure generation, the growth rates of the phases in X, Y, and Z directions are considered equal.

In this study, different cathode microstructures possessing the same voxel size, which have been proven for real cathode microstructure, are compared [9]. Figure 1 demonstrates a realized cathode macrostructure characterized by a voxel size of $150 \times 150 \times 150$ (RVE¹).

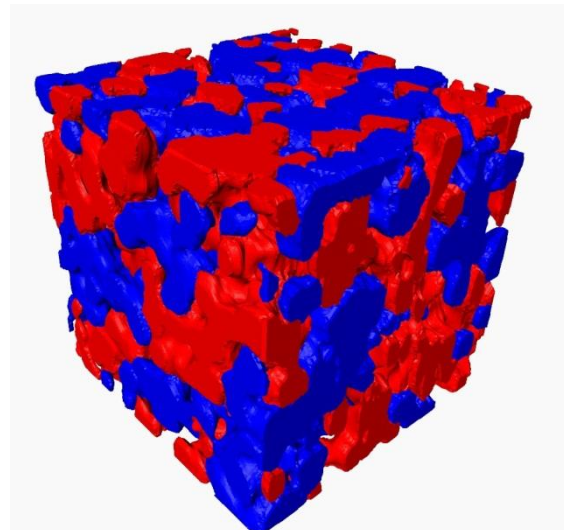


Fig. 1. A model of a realized cathode of SOFC

3. Diffusivity

In a fuel cell system, continuous fuel and oxidant supply is crucial to produce electricity. In SOFC, the movement of the species and reactant is called mass transport. Here, the major part of mass transport is related to the transport of oxygen ions in the electrolyte, which is affected by the potential gradient. However, the uncharged gases are

¹ Representative Volume Element

not influenced by the potential gradient and depend upon diffusion and convection. Convection occurs only in the inlet and outlet channels on a millimeter and centimeter scale; nevertheless, in the electrode, gas transport is most often controlled by diffusion.

As shown in Fig. 2a, in the macro-channels, the presence of very few numbers of molecules near the walls get blocked due to their impacts upon the walls, and the gas molecules diffuse freely. However, in the porous media as shown in Fig. 2b, the gas species diffuse onto the pores with nano- to micro-scales and the number of molecules near the pore walls increases dramatically. Hence, the interaction of the gas molecules with the walls cannot be ignored.

Three diffusion mechanisms occur in the porous media, including molecular diffusion, viscous diffusion, and Knudsen diffusion, which depending on the inherent microstructure and characterization of gas species enables only one of them to occur. To determine the proper mechanism, the Knudsen number (Kn) is typically used. The K_n is calculated from the ratio of the mean free path of the gas to the pore size of the electrode, as seen in Eq.1 [22].

$$k_n = \frac{\lambda}{d_p} \quad (1)$$

where d_p is the pore diameter, and λ is the gas mean free path, which can be calculated using Eq.2:

$$\lambda = \frac{k_B T}{\sqrt{2} p \pi d_g^2} \quad (2)$$

where d_g is the effective diameter of a gas molecule, P is the gas pressure, T is the gas temperature (K) and k_B is the Boltzmann constant (1.3807×10^{-23} J/K). Collisions between the porous electrode and gas molecules are more significant than those between the gas molecules when the K_n is considerably greater than 10; hence, Knudsen diffusion plays a key role in diffusion. If the Kn value is much less than 0.1, collisions and

interactions between the gas molecules become significant and the Knudsen diffusion can be ignored, as compared with molecular diffusion and viscous diffusion. In SOFC, because the temperature and diameter of the gas molecules are constant in the anode and cathode, the pore diameter becomes the determining parameter for the selection of the correct diffusion mechanism.

The gas pathway or channel tortuosity also significantly affects the diffusion duration of the gas transport. The effect of the tortuosity factor on the diffusivity property is indicated in the formula below (Eq.3):

$$D^{eff} = \frac{\phi}{\tau} D \quad (3)$$

where ϕ is porosity, τ is tortuosity, D and D^{eff} are the binary diffusivity of the gas and effective binary diffusivity of gas, respectively [23].

The new released (2013) Avizo Xlab thermo utilizes the voxel as the volume element. With such an approach, the generation of a new volume mesh is eliminated, although all the calculations need to be performed on a larger number of sample cells. Simulation of heat transfer was done on the pore network and effective thermal conductivity, and hence the k_{eff} of the model was obtained. Then the tortuosity factor based on Eq.4 was calculated [24].

$$\tau = \phi \frac{K_{bulk}}{K_{eff}} \quad (4)$$

4. Electric Conductivity

When the electric charges influenced by an electric field are transported through the electrode, the electrical conduction produces free ions which transmit the electrical energy via an electrolyte. Electrical conduction via a homogeneous material is described by Ohm's law (Eq.5):

$$\vec{j} = -\sigma \vec{\nabla} \vartheta \quad (5)$$

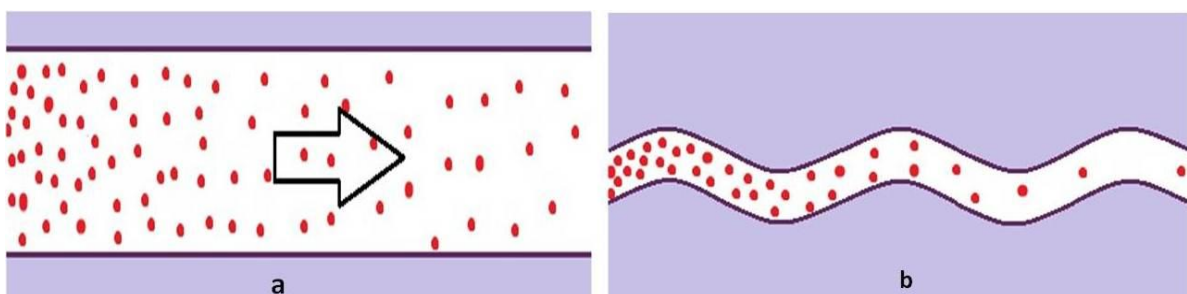


Fig. 2. Gas diffusion (a) in free spaces and (b) in the porous media.

where \vec{j} is the current density, σ is the electrical conductivity of the material and θ is the electrical potential.

A constant electric potential difference is imposed upon two different faces of a porous model to simulate the Formation Factor Experiment Simulation module. Electric insulators are adopted to enclose the other faces. The input and output current fluxes become equal when the final state is achieved, and the apparent electric conductivity is evaluated by using Eq.6 and Ohm's law on the entire volume.

$$\frac{j_{total}}{S} = \sigma \frac{V_{in} - V_{out}}{L} \quad (6)$$

where j_{total} is the total electrical flux going through the input face, S is the area of the input face, σ is the electrical conductivity of the material, V_{in} and V_{out} are the input and output imposed potentials respectively and L is the material sample length. The j_{total} which is the total electric flux through the input face, can be calculated by Eq.7:

$$j_{total} = \int_S -\sigma_{solution} \vec{\nabla} v \cdot \vec{ds} \quad (7)$$

where $\sigma_{solution}$ is the electric conductivity of the free solution. The inverse of the formation factor is related to the electric conductivity. Furthermore, the dimensionless electrical conductivity tensor can be calculated as described in Eq.8.

$$\epsilon \frac{\vec{\sigma}}{\sigma_{solution}} = \epsilon \left(\vec{I} + \frac{1}{v_f} \int_{S_{fs}} \overrightarrow{n_{fs}} \vec{b} ds \right) \quad (8)$$

where ϵ is the porosity, $\sigma_{solution}$ is the solution electrical conductivity, V_f is the volume of the fluid, S_{fs} is the area of the fluid-solid interface and $\overrightarrow{n_{fs}}$ is the normal to the fluid-solid interface directed from the fluid to the solid phase [23].

5.Mechanical Properties

One of the vital factors that controls the life cycle of the SOFC is the mechanical properties of the cathode. By increasing the cathode strength, especially for specific types of SOFCs that the cathode supports, the cell

electrolyte and anode, the life cycle of the SOFC and consequently, the cost will be decreased. The elastic properties of YSZ and LSM are shown in Table 1.

The porosity includes the gas phases which are completely different from its adjacent solid phases (YSZ and LSM). Therefore, the percentage of porosity exerts a significant effect on the mechanical properties of the cathode [25-30]. By applying the finite-element method, Young's modulus and Poisson's ratio of the cathode in the X, Y and Z directions have been calculated. In order to evaluate their mechanical properties, one surface of the simulated RVE of cathode was fixed in every direction and then a displacement was applied on the opposite face. Using a python code in the Abaqus software, the degree of stress and also the volume of all the elements in the model were extracted. The following equations were utilized to calculate the Young's modulus and Poisson's ratio of the cathode:

$$\sigma_{xx} = \frac{\sum_{i=1}^n \sigma_{xx} \times v_i}{\sum_{i=1}^n v_i} \quad (9)$$

$$\sigma_{yy} = \frac{\sum_{i=1}^n \sigma_{yy} \times v_i}{\sum_{i=1}^n v_i} \quad (10)$$

$$\sigma_{zz} = \frac{\sum_{i=1}^n \sigma_{zz} \times v_i}{\sum_{i=1}^n v_i} \quad (11)$$

$$[\sigma] = C[\epsilon] \quad (12)$$

$$S = C^{-1}$$

$$S = \begin{bmatrix} 1 & -v_{yx} & -v_{yz} & 0 & 0 & 0 \\ \frac{v_{xy}}{E_x} & 1 & -\frac{v_{zy}}{E_x} & 0 & 0 & 0 \\ \frac{v_{xy}}{E_x} & \frac{1}{E_y} & -\frac{v_{zy}}{E_x} & 0 & 0 & 0 \\ \frac{v_{xy}}{E_x} & -\frac{v_{yz}}{E_x} & \frac{1}{E_z} & \frac{2(1+v_{yz})}{E_y} & 0 & 0 \\ 0 & 0 & 0 & 0 & \frac{1}{G_{xy}} & 0 \\ 0 & 0 & 0 & 0 & 0 & \frac{1}{G_{xy}} \end{bmatrix}$$

where σ is the tension, ϵ is the strain and C is the stiffness matrix.

Table 1.The elastic properties of YSZ and LSM

Material	Young modulus (E)	Poisson's ratio (v)
LSM	40 Gpa	0.25
YSZ	215 Gpa	0.23

6.Results and Discussion

The Three Phase Boundary Length (TPBL) of all the realized structures is calculated via a code [31]. As shown in Fig. 3, the TPBL value of the sample having a porosity of 28% has increased moderately and is almost reaching 31% to maximum value. From 31 to 34% porosity, the TPBL value dropped slightly but after 34%, a dramatic decline in the TPBL values is observed. According to Fig. 2, the best porosity value for the cathode with the highest TPBL hovers between 31 and 34%. This implies that the optimum porosity for the cathode microstructure, with a maximum TPBL density is around 31%. According to an experimental study, 34%

porosity is considered the best porosity value for the cathode microstructure [32].

Electric conductivity was studied using the Avizo Fire commercial software. As Fig. 4 demonstrates the porosity value of the electric conductivity decreased dramatically between 31 and 34%. Increasing the porosity from 28 to 31% and also from 34 to 43% exerted only a minor impact on the value of the electrical conductivity. According to the results, the electrical conductivity clearly changed between 31 and 34% porosity. Hence, for increasing the electric conductivity and following the electrochemical reactions of the cathode, it was crucial to observe the porosity factor. Designing a cathode electrode with a porosity value below 34% will enhance cell performance:

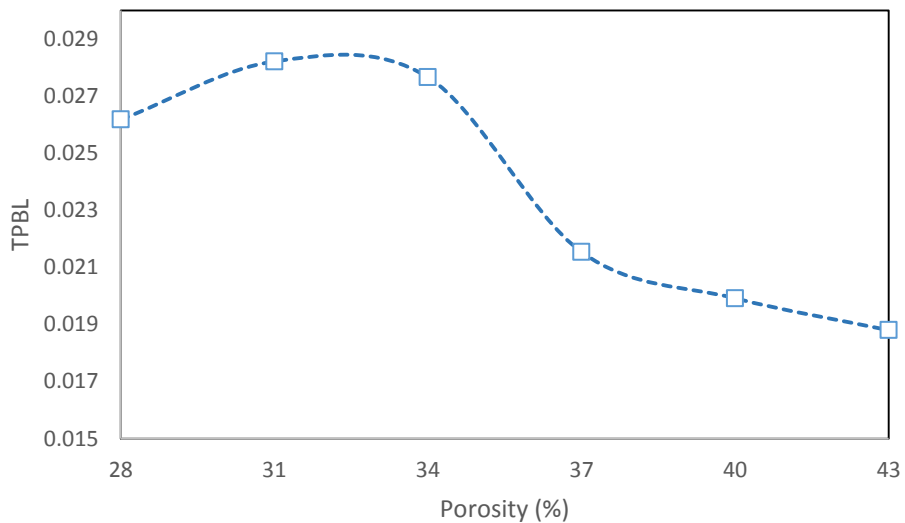


Fig. 3. The value of TPBL in different porosities

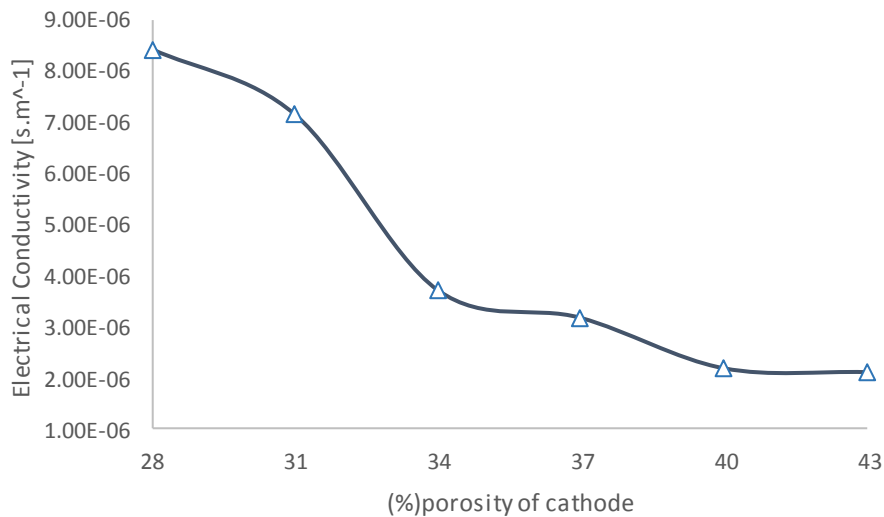


Fig. 4. Electrical conductivity of LSM phase vs porosity of cathode

As depicted in Fig. 5 the tortuosity of the gas pathway in the cathode structure is influenced by the porosity factor. The pathway tortuosity and porosity value reveal an approximately linear relationship. A smooth decrease in the tortuosity of the pore phase can be observed by an increasing porosity value. According to the results, increasing the porosity of a structure besides increasing the gas flow pathways, can decrease the tortuosity of the pore phase and thus ultimately enhance the gas diffusivity. Also, the tortuosity values given in Fig. 5 are normalized.

As Fig. 6 reveals, the Young's modulus in the X, Y and Z directions is decreased by increasing the porosity. The Young's

modulus of the cathode in the main directions is decreased to 56% when the porosity is enhanced from 28 to 43%.

The Poisson's ratio of the cathode gets reduced as the porosity is increased but as shown in Fig. 7 the rate of its variation is less than the variation of the Young's modulus in the previous Figure.

7. Conclusion

The 3-D reconstruction of the cathode of the SOFC based on the Monte Carlo approach has been performed. Six microstructures having different porosities realized as well as TPB densities, mechanical behaviors, pore tortuosity and electrical conductivity have been studied and compared. It has been

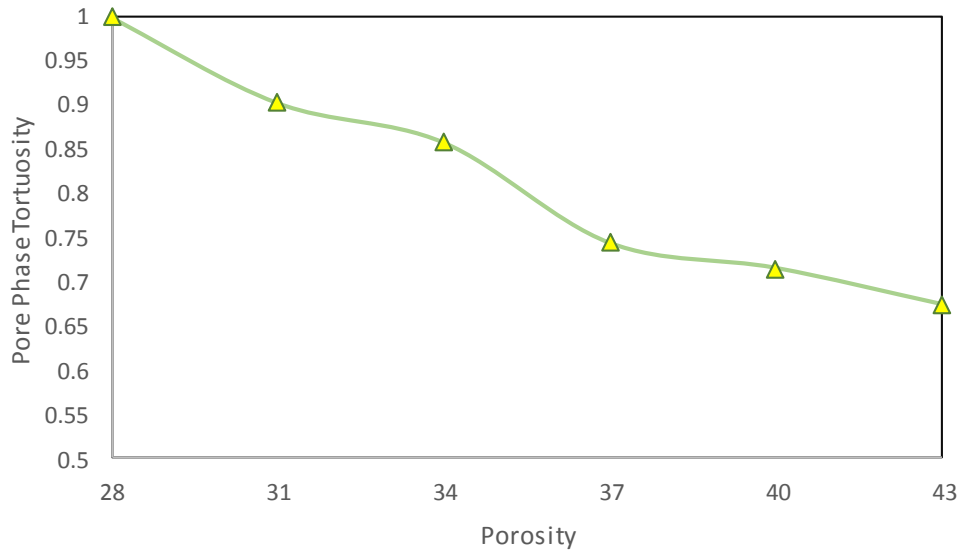


Fig. 5. Effect of Cathode porosity on the tortuosity of the gas pathway.

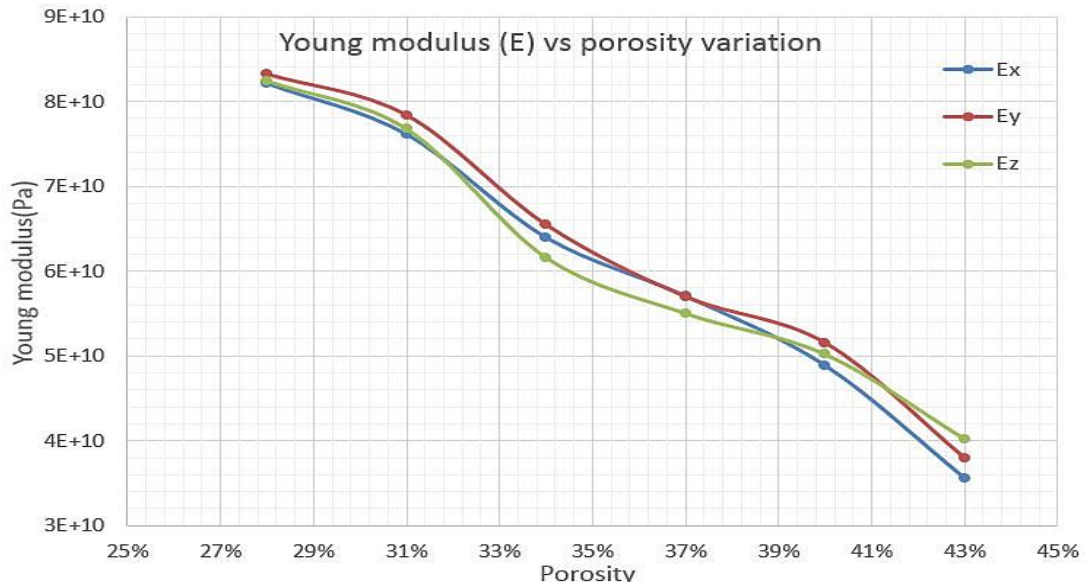


Fig. 6. The effects of porosity variation on Young's modulus

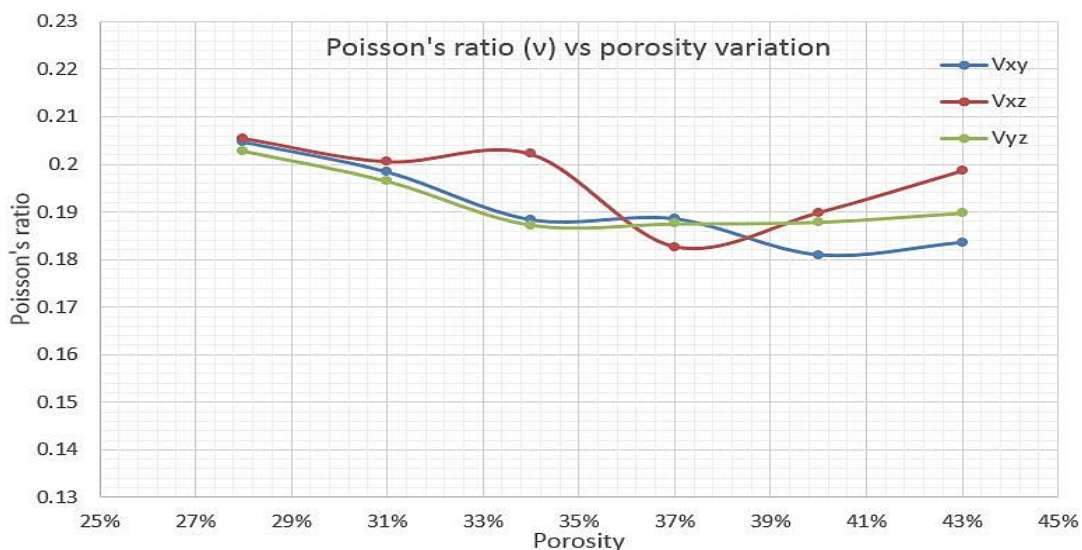


Fig. 7. The effects of porosity variation on Poisson's ratio

performed. Six microstructures having different porosities realized as well as TPB densities, mechanical behaviors, pore tortuosity and electrical conductivity have been studied and compared. It has been shown that the porosity of a microstructure between 31 and 34% has the maximum TPBL value, as well as the maximum variation in electric conductivity. Also, any increase in the porosity results in a decrease in the tortuosity of the pore phase which can facilitate the gas transport in the microstructure. The mechanical properties were calculated and the Young's modulus and Poisson's ratio versus porosity among the six models were obtained.

References:

- [1] Farhad S., Hamdullahpur F., AIChE Journal, 58 (2012) 1248-1261.
- [2] Singhal S., High-Temperature Solid Oxide Fuel Cells: Fundamentals, Design and Applications, Elsevier, (2003).
- [3] Deseure J., Bultel Y., Dessemond L., Siebert E., Electrochimica Acta, 50 (2005) 2037-2046.
- [4] Lehnert W., Meusinger J., Thom F., Journal of Power Sources, 87 (2000) 57-63.
- [5] Choi J.H., Jang J.H., Oh S.M., Electrochimica Acta, 46 (2001) 867-874.
- [6] Murray E.P., Tsai T., Barnett S.A., Solid State Ionics, 110 (1998) 235-243.
- [7] McIntosh S., Adler S.B., Vohs J.M., Gorte R.J., Electrochemical and Solid-State Letters, 7 (2004) A111-A114.
- [8] Wilson J.R., Cronin J.S., Duong A.T., Rukes S., Chen H.-Y., Thornton K., Mumm D.R., Barnett S., Journal of Power Sources, 195 (2010) 1829-1840.
- [9] Yokokawa H., Tu H., Iwanschitz B., Mai A., Journal of Power Sources, 182 (2008) 400-412.
- [10] Wilson J.R., Cronin J.S., Duong A.T., Rukes S., Chen H.-Y., Thornton K., Mumm D.R., Barnett S., Journal of Power Sources, 195 (2010) 1829-1840.
- [11] Kim J.-D., Kim G.-D., Moon J.-W., Lee H.-W., Lee K.-T., Kim C.-E., Solid State Ionics, 133 (2000) 67-77.
- [12] Kim J.-D., Kim G.-D., Moon J.-W., Park Y.-i., Lee W.-H., Kobayashi K., Nagai M., Kim C.-E., Solid State Ionics, 143 (2001) 379-389.
- [13] Liu Y., Compson C., Liu M., Journal of Power Sources, 138 (2004) 194-198.
- [14] Kim J.W., Virkar A.V., Fung K.Z., Mehta K., Singhal S.C., Journal of the Electrochemical Society, 146 (1999) 69-78.
- [15] Janardhanan V.M., Deutschmann O., Zeitschrift für Physikalische Chemie, 221 (2007) 443-478.
- [16] Kenney B., Karan K., Solid State Ionics, 178 (2007) 297-306.
- [17] Dong D., Gao J., Liu X., Meng G., Journal of Power Sources, 165 (2007) 217-223.
- [18] Bi L., Tao Z., Sun W., Zhang S., Peng R., Liu W., Journal of Power Sources, 191 (2009) 428-432.
- [19] Wilson J.R., Barnett S.A., Electrochemical and Solid-State Letters, 11 (2008) B181-B185.
- [20] Matsuzaki Y., Yasuda I., Solid State Ionics, 152 (2002) 463-468.
- [21] Vaidya S., Kim J.-H., Journal of Power Sources, 225 (2013) 269-276.

- [22] Kenney B., Valdmanis M., Baker C., Pharoah J., Karan K., Journal of Power Sources, 189 (2009) 1051-1059.
- [23] Avizo XLab Pack User's Guide, in, pp. 507-582.
- [24] Cooper S.J., Kishimoto M., Tariq F., Bradley R.S., Marquis A.J., Brandon N.P., Kilner J.A., Shearing P.R., ECS Transactions, 57 (2013) 2671-2678.
- [25] Amani Hamedani H., Baniassadi M., Sheidaei A., Pourboghrat F., Garmestani H., Three-Dimensional Reconstruction and Microstructure Modeling of Porosity-Graded Cathode Using Focused Ion Beam and Homogenization Techniques, Fuel Cells 14 (1), 91-95.
- [26] Tabei SA., Sheidaei A., Baniassadi M., Pourboghrat F., Garmestani H., Microstructure Reconstruction and Homogenization of Porous Ni-YSZ Composites for Temperature Dependent Properties, Journal of Power Sources 235, 74-80.
- [27] Baniassadi M., Mortazavi B., Hamedani HA., Garmestani H., Ahzi S., Three-Dimensional Reconstruction and Homogenization of Heterogeneous Materials Using Statistical Correlation Functions and FEM, Computational Materials Science 51 (1), 372-379.
- [28] Hamedani HA., Baniassadi M., Khaleel M., Sun X., Ahzi S., Ruch D., Microstructure, Property and Processing Relation in Gradient Porous Cathode of Solid Oxide Fuel Cells Using Statistical Continuum Mechanics, Journal of Power Sources 196 (15), 6325-6331.
- [29] Baniassadi M., Garmestani H., Li DS., Ahzi S., Khaleel M., Sun X., Three-Phase Solid Oxide Fuel Cell Anode Microstructure Realization Using Two-Point Correlation Functions, Acta Materialia 59 (1), 30-43.
- [30] Baniassadi M., PhD Dissertation, University of Strasbourg, Development of a Multiscale Approach for the Characterization and Modeling of Heterogeneous Materials, Application to Polymer Nanocomposites (2011).
- [31] Mazroui M., Baniassadi M., Jamali J., Abrinia K., in: 3rd Hydrogen and Fuel Cell Conference, Tehran, (2015).
- [32] Nelson G.J., Harris W.M., Lombardo J.J., Izzo J.R., Chiu W.K., Tanasini P., Cantoni M., Comninellis C., Andrews J.C., Liu Y., Electrochemistry Communications, 13 (2011) 586-589.